

Cite this article as: Liu Yanfeng, Wang Xianhui, He Xuan, et al. Microstructure and Arc Erosion Behavior of AgSnO₂TiB₂ Contact Material Prepared by Different Methods[J]. Rare Metal Materials and Engineering, 2022, 51(04): 1164-1171.

ARTICLE

Microstructure and Arc Erosion Behavior of AgSnO₂TiB₂ Contact Material Prepared by Different Methods

Liu Yanfeng^{1,2}, Wang Xianhui¹, He Xuan², Wan Mengyu², Su Yanning², Chi Xiaotong², Chen Tingting², Miao Yu², Wang Lizhao²

¹ School of Materials Science and Engineering, Xi'an University of Technology, Xi'an 710048, China; ² School of Chemical Engineering and Modern Material, Shangluo University, Shangluo 726000, China

Abstract: The AgSnO₂TiB₂ composite powders were synthesized by the ball milling, soluble starch template and filter paper template methods, and subsequently consolidated by spark plasma sintering (SPS). The physical properties and arc erosion behavior of Ag4wt%-SnO₂4wt%TiB₂ contact materials were investigated. The results reveal that the spatial domain-limiting effects of the template can remarkably improve the dispersion of the reinforcements in the Ag matrix, and then electrical conductivity and hardness of Ag4wt%-SnO₂4wt%TiB₂ contact materials are increased. As compared to the ball milling, the electrical conductivity of Ag4wt%SnO₂4wt%TiB₂ composites fabricated by filter paper template and starch template method is increased by 12.18 and 9.60 times, while the microhardness is increased by 17.10% and 33.94%, respectively. The filter paper template is more beneficial for the uniform dispersion of SnO₂ and TiB₂, which can alleviate concentrated arc erosion and reduce splash, thereby exhibiting better arc erosion resistance.

Key words: template method; contact material; physical properties; arc erosion characteristic

The electrical contact is the core component of various AC and DC contacts, relays, circuit breakers. It is responsible for switching on, conducting current and switching off, and its performance directly determines the operation reliability and stability of the electrical apparatus^[1,2]. Therefore, the contact materials should possess good thermal conductivity, excellent welding and arc erosion resistance along with low and stable contact resistance^[3]. Though AgCdO has the outstanding electrical and processing performance, the toxic Cd vapor decomposed under high-temperature conditions is detrimental to the environment and humanity health^[4]. The AgSnO₂ contact material can be comparable to the AgCdO in a certain degree. However, because of the poor wettability between Ag and SnO₂, it is easier to cause the aggregation of SnO₂ particles on the contact surface, resulting in high temperature rise and large contact resistance, thereby affecting the reliability and safety of the electrical system^[5-7].

Thus far, extensive researches have demonstrated that the dispersion of the reinforcement phase significantly influences the electrical properties of the contact materials^[8,9]. Wang et al^[10] revealed that the AgSnO₂ contact materials with uniform microstructure exhibit supreme arc dispersion and arc erosion resistance characteristics. Akbi et al^[11] reported that the uniform dispersion of submicron or nanometer Ni particles enhances the arc erosion resistance of Ag-base composites. Moreover, the nanocrystallization of the second phase oxide dramatically enhances the arc erosion resistance of AgSnO₂ contact material^[12]. However, it is quite difficult to achieve the distribution uniformity of the nano-SnO₂ reinforcement in the Ag matrix via the internal oxidation or conventional powder metallurgy method^[13]. More efforts have been made to improve the dispersion of nanoparticles by various methods, such as chemical co-precipitation method^[14], mechanical alloying^[15], in-situ synthesis^[16], reaction synthesis^[17], sol-gel

Received date: January 04, 2022

Foundation item: National Natural Science Foundation of China (51971173); National College Students Innovation and Entrepreneurship Training Program (S202011396002, S202011396005); Shaanxi College Students Innovation and Entrepreneurship Training Program (S202111396030); Shangluo Science and Technology Innovation Team (SK2019-75); Funded by Shaanxi Provincial Department of Education (20JK0618); Key Research and Development Plan Project of Shaanxi Province (2022GY-379)

Corresponding author: Wang Xianhui, Professor, School of Materials Science and Engineering, Xi'an University of Technology, Xi'an 710048, P. R. China, Tel: 0086-29-82312185, E-mail: xhwang693@xaut.edu.cn

Copyright © 2022, Northwest Institute for Nonferrous Metal Research. Published by Science Press. All rights reserved.

method^[18], and template method. Among these methods, the template method possesses the characteristics of good dispersion, easy-regulated structure and inexpensive cost^[19-22]. However, though these researches have achieved the well distribution of the reinforcement and the improvement in physical and mechanical properties of the AgSnO₂ contact material synthesized by template methods, few literatures have been reported on the electrical behavior so far.

During long-term service, the AgSnO₂ contact material exhibits high temperature rise and large contact resistance due to non-conductive properties of SnO₂^[23]. To compensate for these shortcomings, TiB₂ ceramics with good thermal and electrical conductivity were incorporated in the AgSnO₂ contact materials in this study, and the AgSnO₂TiB₂ composite powders were synthesized by three different methods including filter paper template, soluble starch template method and ball milling, followed by consolidation via SPS to fabricate the bulk contact materials. The resulting materials were examined to determine the phase constituents, microstructure and physical properties, and the arc erosion behavior was studied by the electrical contact tests. The purpose is to clarify the effect of TiB₂ incorporation and microstructure on the physical properties and electrical characteristic of the AgSnO₂TiB₂ contact material.

1 Experiment

The AgSnO₂TiB₂ composite powders were synthesized by filter paper template, the soluble starch template method and ball milling; in order to describe conveniently, the three different composite powders were denoted as composite powders A, composite powders B, composite powders C, respectively. As for synthesis of the composite powders A, the details are given as follows. TiB₂ (99.9%, 3~5 μm) and SnO₂ powder (99.9%, 50 nm) were weighed according to the mass ratio of 4:4 and subsequently suspended in 5% ethanol water solution to obtain TiB₂ and SnO₂ nanoparticle suspension, and then 1 mol/L AgNO₃ solution was added, followed by the magnetic stirring for 8 h. Afterwards, the sufficient amount of fragmented ash-free filter paper was fully impregnated in the above mixed solution to adsorb the solution by the filter paper completely. Finally, the loaded filter paper template was dried and calcined at 873 K for 240 min in a muffle furnace to remove the template, and AgSnO₂TiB₂ composite was obtained.

As for the composite powders B, the synthesis method is given below. First, 10 g soluble starch was added to 400 mL deionized water, which was slowly heated to 373 K and held for 10 min in a water bath and then cooled to 343 K by magnetic stirring to obtain the starch template solution. Subsequently, 0.42 g TiB₂ and 0.42 g SnO₂ were added into the solution in turn by magnetic stirring for 10 min. Further, 1 mol/L AgNO₃ solution was slowly added to the above starch template solution, accompanied by magnetic stirring for 30 min. Finally, the mixture was fully dried at 333 K in a drying cabinet and calcined at 873 K for 240 min in a muffle furnace to obtain AgSnO₂TiB₂ composite powder.

The ball milling was performed on a QQM-Y/B planetary ball mill. Ag (99.9%, 500 nm), SnO₂ and TiB₂ powders with a mass ratio of 92:4:4 were mixed with the agate ball:powders mass ratio of 15:1 at 300 r/min for 240 min to obtain AgSnO₂TiB₂ composite powder.

These AgSnO₂TiB₂ composite powders were sintered at 1023 K for 5 min under a pressure of 40 MPa in a LABOX-330 SPS furnace.

The relative density and electrical conductivity were determined by a FA1104J density measuring instrument and a Sigma 2008B/C digital eddy current conductivity meter, respectively. The hardness test was conducted on a HV-120 Vickers tester at a load of 5000 g for 30 s, and the hardness value was an average of five measured results. The resulting materials were machined to obtain the electrodes with the dimensions of Φ3.8 mm×8 mm. The arc erosion testing was performed for 5000 times under DC 16 A/24 V in the JF04C electrical contact material testing system. The phase constituents of the composite particles were analyzed by X-ray diffractometer (XRD). The eroded morphology and element distribution were examined by a JSM-6700F scanning electron microscope (SEM) equipped with an energy dispersion spectrometer (EDS). The mass changes of electrodes were detected with a FA1104J electrical balance.

2 Results and Discussion

2.1 Phase analysis and morphology

Fig. 1 shows the XRD patterns of AgSnO₂TiB₂ composite powders obtained by three different methods. Obviously, all composite powders are composed of Ag, TiB₂ and SnO₂ without the presence of other impurity, suggesting that the template and impurities can be removed completely after calcination. In addition, the resulting composite powder A presents a lower diffraction peak intensity and a greater peak width, indicating that the composite powder has a smaller granularity.

Fig. 2 shows the morphologies of the AgSnO₂TiB₂ composite powder prepared by different methods. Evidently, there is a serious agglomeration of Ag, SnO₂ and TiB₂

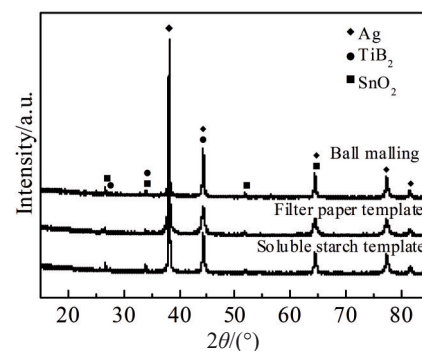


Fig.1 XRD patterns of AgSnO₂TiB₂ composite powder synthesized by ball milling, filter paper template, and soluble starch template

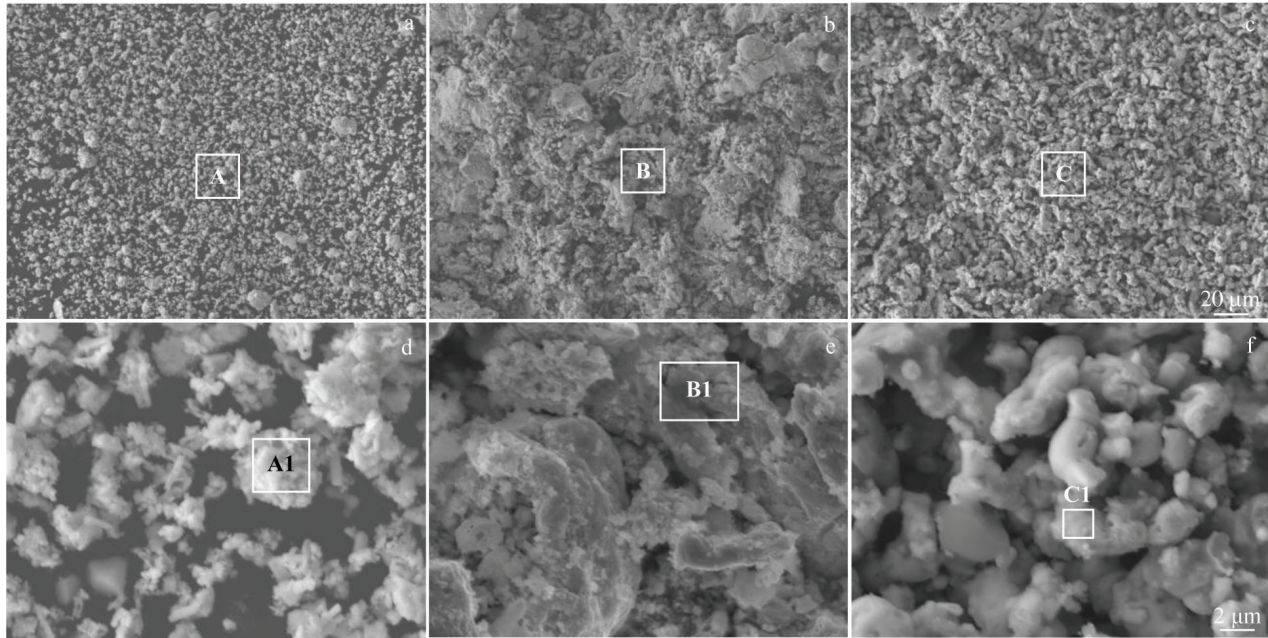


Fig.2 SEM micrographs of $\text{AgSnO}_2\text{TiB}_2$ composite powder synthesized by ball milling (a, d), filter paper template (b, e), and soluble starch template (c, f)

nanoparticles in the composite powder C (Fig.2a and Fig.2d). The composite powder A has obvious patches (Fig.2b and Fig.2e), which is related to the mesh pore structure of the filter paper template. It is indicated that the inherent structure of the filter paper template will also be inherited to the composite powder after impregnation, adsorption, drying and calcination. As seen from Fig. 2c and Fig. 2f, no obvious agglomeration occurs for the composite powder B. EDS results of the region A1, B1, C1 in Fig.2d~2f are shown in Table 1, which reveals that the dispersion of reinforcement SnO_2 and TiB_2 can be improved by using the filter paper as template.

2.2 Properties

The relative density, electrical conductivity and hardness of the resultant composites are presented in Fig.3. As compared to the ball milling, the relative density and hardness of the resultant composite prepared by filter paper template method are increased by 33.18% and 17.10%, respectively; while the relative density and hardness of the resultant composite prepared by starch template method are enhanced by 24.53% and 33.94%, respectively; in particular, the electrical conductivity is dramatically increased by 12.18 and 9.60 times, respectively.

Table 1 EDS results of regions A1, B1, C1 marked in Fig.2d~2f, respectively (wt%)

Element	A1	B1	C1
Ag	76.92	65.56	58.01
Ti	1.68	4.40	1.19
Sn	9.33	7.79	6.39
O	12.07	22.25	34.41

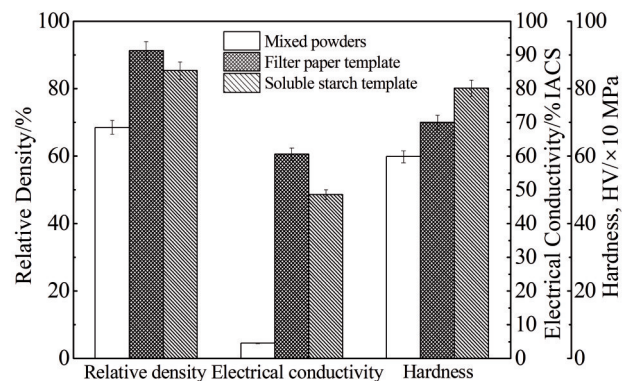


Fig.3 Relative density, electrical conductivity and hardness of $\text{AgSnO}_2\text{TiB}_2$ composites prepared by different methods

2.3 Variation of arc energy and duration

The distribution curves of arc-energy and arc-duration per 100 operations are shown in Fig. 4a~4c and Fig. 4d~4f, respectively. Obviously, there are similar changing trend during 5000 operations. As shown in Fig. 4a and Fig. 4d, the arc energy and arc-duration have a larger fluctuation for the resultant composite prepared by ball milling. However, there is relative stability in 2300 to 4000 times operation. The average make-arc-energy and make-arc-duration are 21.38 mJ and 1.45 ms, while the average break-arc-energy and break-arc-duration are 5.0 mJ and 0.34 ms, respectively. For the resultant composite fabricated by filter paper template, both the make-arc-energy and make-arc-duration are stable, which are approximately 1.4 mJ and 0.03 ms, respectively. Furthermore, compared with the composite prepared by the ball milling, the break-arc-energy and break-arc-duration are

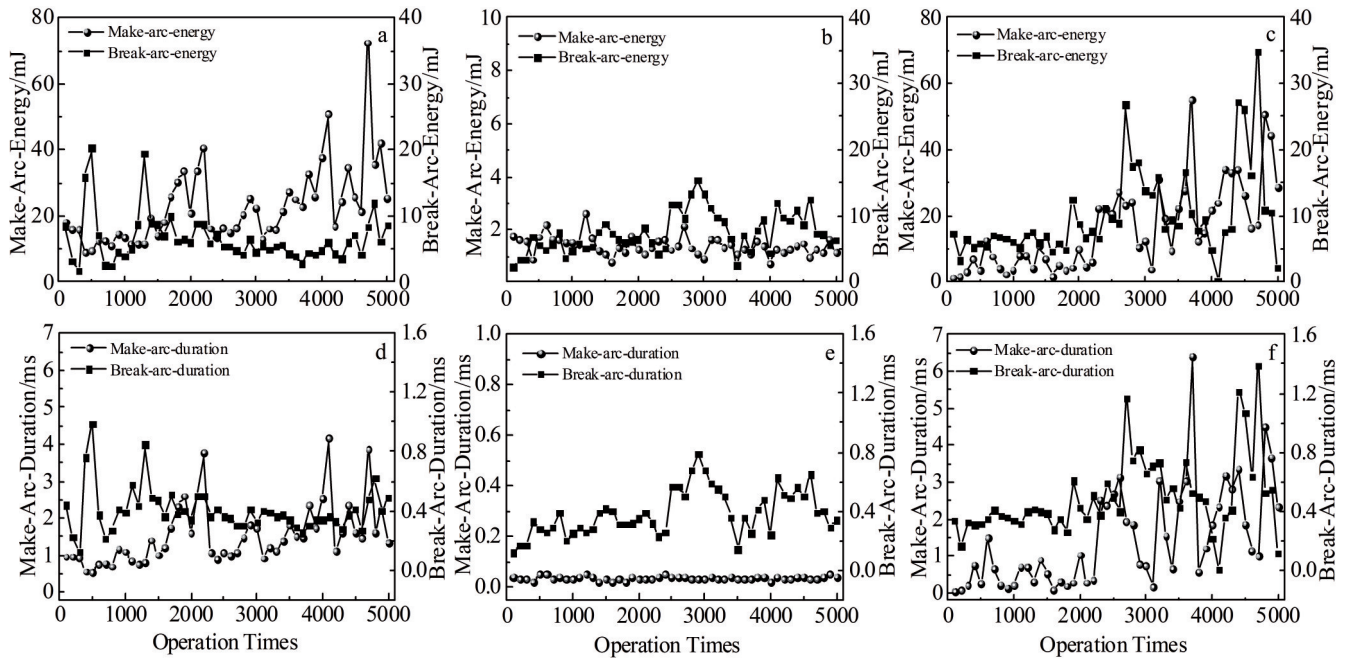


Fig.4 Variation of arc-energy and arc-duration with operation times for the $\text{AgSnO}_2\text{TiB}_2$ composites: (a, d) ball milling; (b, e) filter paper template; (c, f) soluble starch template

more stable during the first 2400 times operation, followed by the occurrence of fluctuation (Fig. 4b and Fig. 4e). For the resultant material fabricated by the soluble starch template, the make-arc-energy and make-arc-duration are stable during the first 2200 times operation, and the break-arc-energy and break-arc-duration are also stable during the first 2600 times operation. Subsequently, slight increase and dramatical fluctuation develop in both cases (Fig. 4c and Fig. 4f). It suggests that the filter paper template method is more conducive to the increase of the arc erosion resistance of the $\text{AgSnO}_2\text{TiB}_2$ contact material.

2.4 Eroded morphologies

The eroded morphologies of the $\text{AgSnO}_2\text{TiB}_2$ composite prepared by the ball milling are shown in Fig. 5. Clearly, there is a large erosion pit at the center of the anode (Fig. 5a), indicating a serious material transfer from anode to cathode. Typical arc erosion features of splash silver and woven mesh are also found at the center and edge of the erosion area (regions B and C marked in Fig. 5a). Due to the combined action of arc heat and the Lorentz force, the kinetic energy of molten silver in the molten pool exceeds the surface tension force, thus causing the flow of silver and even splashing in severe cases. The splash silver results in the formation of circular silver particles during solidification (Fig. 5b). These rapidly solidified Ag causes the occurrence of woven mesh morphology under multi-frequency make-break operations, and the longitudinal extension of the morphology is closely related to the molten bridge fracture between the contact pairs (Fig. 5c). From Fig. 5d, the cathode exhibits severe arc erosion morphology along with deeper and larger erosion pits as compared to the anode. Meanwhile, coarse cracks, visible

holes and Ag beads formed by droplet splash can also be observed. Since the arc energy causes more Ag to melt, a large amount of oxygen can be absorbed until it is saturated in the molten Ag pool^[8]. Nevertheless, the excessive oxygen can escape during solidification, giving rise to the formation of the pores on the contact surface (Fig. 5e). From the EDS results of the region F marked in Fig. 5e, SnO_2 agglomerates on the surface of the contacts, which can be attributed to the poor wettability between Ag and SnO_2 and the low density of SnO_2 .

Fig. 6 shows the eroded morphologies of the $\text{AgSnO}_2\text{TiB}_2$ composite prepared by the filter paper template. As seen from Fig. 6a, erosion area is quite small on the anode (approximately 1.76 mm), and the electrode surface is relatively flat without the presence of large pits. Fig. 6b shows the presence of large areas of honeycomb, starchiness solidification morphology, small number of cracks and pits in the region B. From Fig. 6c, a large number of flow Ag trace, spherical Ag particles, pores and small cracks appear in region C. As determined by the EDS results in region D marked in Fig. 6c, the SnO_2 and TiB_2 present the more uniform dispersion in the Ag matrix without significant aggregation (Fig. 6d, ~6d₄). The chemical composition of region E in Fig. 6c shows a remarkable increase in Ti and Sn content due to the lower density of SnO_2 and TiB_2 than that of Ag. The eroded cathode also has a smaller erosion area, but a deeper corrosion pit is generated close to the erosion center (Fig. 6f). Porous morphology and starchiness consolidation morphology are observed in region G at eroded cathode (Fig. 6g). The EDS line scanning of region H can verify the formation of obvious Sn/Ti-rich and Ag-rich zones. This can be ascribed to the increase of the melt pool viscosity. When the arc acts on the contact surface, Ag in the arc root area rapidly melts,

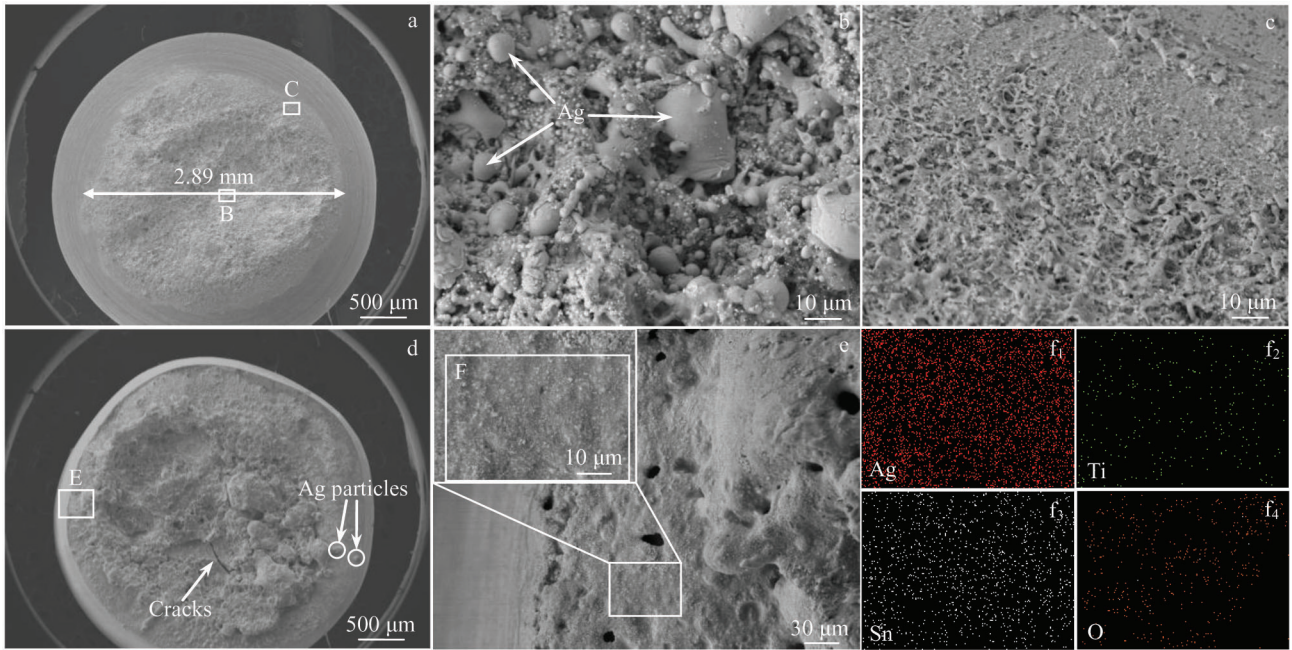


Fig.5 Eroded morphologies of the $\text{AgSnO}_2\text{TiB}_2$ composite prepared by ball milling: (a) eroded anode; (b, c) magnified images of region B and C, respectively; (d) eroded cathode; (e) magnified image of region E in Fig.5d; ($f_1\sim f_4$) EDS element mapping of region F in Fig.5e

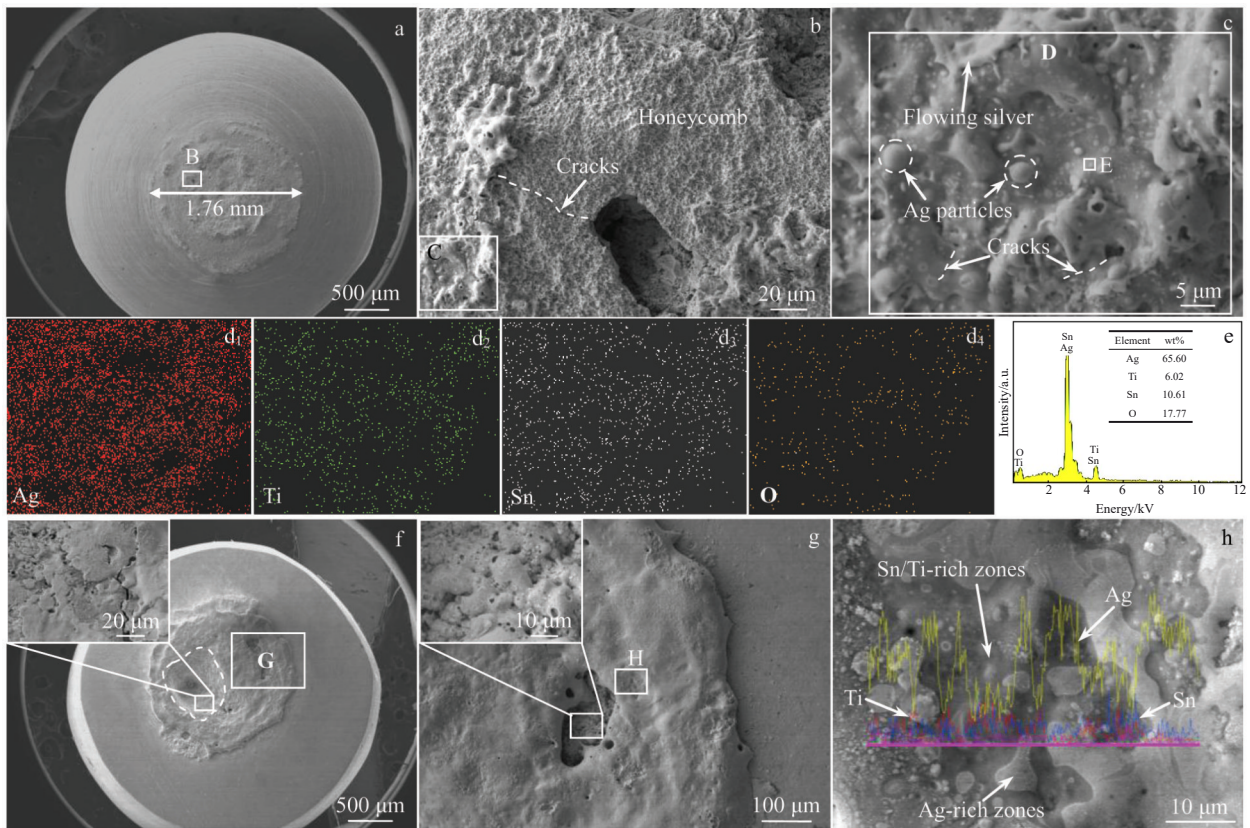


Fig.6 Eroded morphologies of the $\text{AgSnO}_2\text{TiB}_2$ composite prepared by filter paper template: (a) eroded anode; (b) magnified image of region B in Fig.6a; (c) magnified image of region C in Fig.6b; ($d_1\sim d_4$) EDS element mapping of region D in Fig.6c; (e) EDS results of region E in Fig.6c; (f) eroded cathode; (g) magnified image of region G in Fig.6f; (h) EDS line scanning of region H in Fig.6g

evaporates, and solidifies, giving rise to the formation of the Ag droplets on the contact surface. As a result, the $\text{AgSnO}_2\text{TiB}_2$ composite prepared by filter paper template possesses better arc erosion resistance than that prepared by ball milling.

Fig. 7 is the eroded morphologies of the $\text{AgSnO}_2\text{TiB}_2$ composite prepared by soluble starch template. As can be seen from Fig. 7a, there are larger erosion area together with shallower and more dispersed erosion pits, indicating the uniform arc erosion. Fig. 7b and Fig. 7c are the magnified images of the typical erosion morphologies of the eroded anode of area B, C marked in Fig. 7a, respectively. A distinct coral morphology appears (Fig. 7b), whereas cracks, pores, silver beads, and flowing silver trace occur (Fig. 7c). Under the action of multi-frequency arc, the repeated solid-liquid-gas phase transformation occurs on the eroded anode surface. Once a large amount of oxygen is inhaled at the liquid-gas state, the loose aggregation similar to coral islands is generated by rapid solidification, as shown in Fig. 7b. Due to the higher oxygen content in the pores along with coral morphologies, the electrical conductivity, arc mechanical properties, arc erosion resistance will be reduced obviously. Fig. 7d displays the eroded morphology of cathode. It is obvious that there are large holes and flowing silver trace on the eroded surface. From Fig. 7e, large cracks and porous areas can be observed, in region E at the erosion center. The magnified image of the F area at the erosion edge is shown in Fig. 7f. It is visible from Fig. 7f that an overlapping and accumulated lava-like morphology forms, and a large number of pores appear at the edge of the erosion zone. It indicates that arc is more concentrated at the center of the erosion zone, thereby resulting in the transfer of the intermediate Ag to the

marginal.

2.5 Discussions

2.5.1 Properties

The low relative density of the composite prepared by ball milling is related to particle size and sintering process. Rapid sintering induces the melting and evaporation of Ag nanoparticles, thus resulting in the formation of a large number of pores and the decrease in relative density, which enhance electron scattering and reduce the electrical conductivity. However, the spatial domain-limiting effects of the filter paper and the starch template can encapsulate the reinforcement particles in the Ag motif, thereby giving rise to more uniform microstructure. The uniform dispersion and low porosity of the reinforcement can effectively enhance the resistance to external forces. Moreover, the encapsulation structure of the Ag motif to the SnO_2 and TiB_2 reinforcement benefits to the connectivity among Ag particles, thus improving the electrical conductivity, which can be confirmed by the results in Section 2.2.

2.5.2 Arc erosion

When the contact pairs is switch-on or switch-off, arc discharge occurs, during which arc prefers to occur at the phase with low work function^[24]. Since TiB_2 has a larger work function than Ag and SnO_2 (Ag-4.70 eV, SnO_2 -3.54 eV, TiB_2 -5.08 eV)^[25,26], its incorporation will undoubtedly increase the integral work function of the $\text{AgSnO}_2\text{TiB}_2$ contact material, thereby delaying arc generation. Further, the uniform distribution of the reinforcements is favorable for arc dispersion, which can reduce the concentrated arc erosion. Due to the processing conditions and the high surface energy of nanoparticles, it is easy to cause the poor dispersion of TiB_2

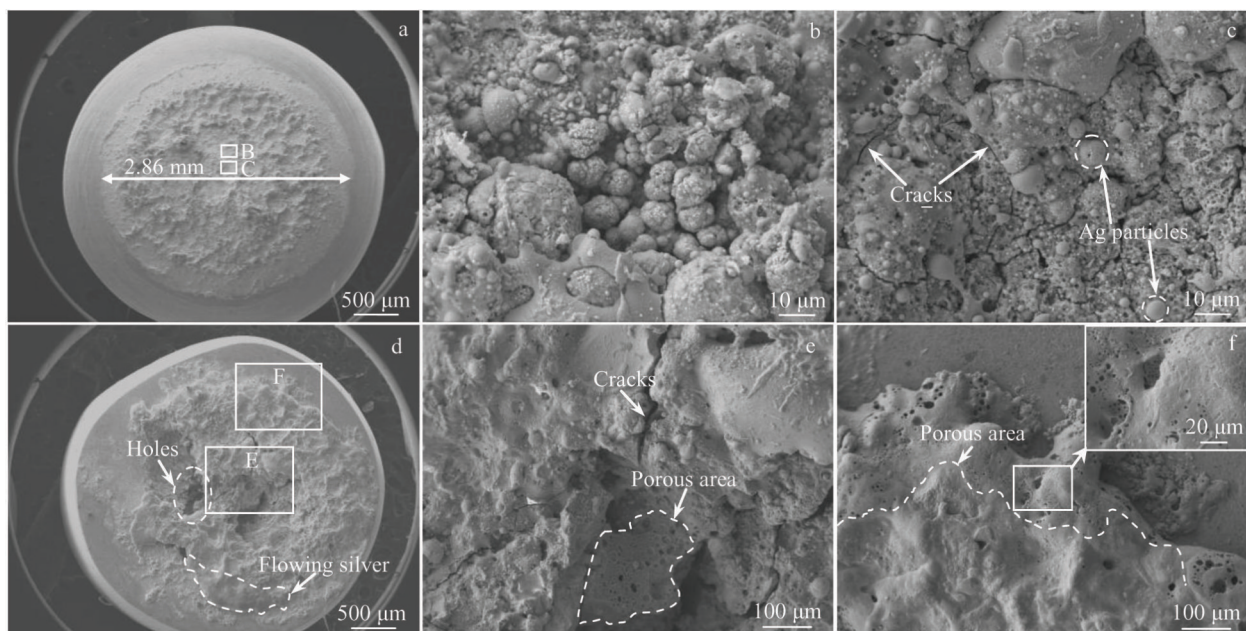


Fig.7 Eroded morphologies of $\text{AgSnO}_2\text{TiB}_2$ composite prepared by soluble starch template: (a) eroded anode; (b) and (c) magnified images of region B and C marked in Fig.7a, respectively; (d) eroded cathode; (e, f) magnified images of region E, F marked in Fig.7d, respectively

and SnO₂ particles in the ball milling. Further, the arcs easily occur in the low work function phase and poor dispersion is prone to cause the arc concentrated erosion, thereby resulting in severe erosion of the contact surface. Moreover, higher arc energy leads to the formation of larger molten pool, causing the increased surface electrical resistance due to the floatation of the lower density SnO₂ (6.95 g/cm³) and TiB₂ (4.52 g/cm³). Since more uniform microstructure can be obtained by filter paper template and starch template, the well-dispersed SnO₂ and TiB₂ can apparently reduce concentrated arc erosion. The similar results are also reported in Ref.[27,28].

2.5.3 Evaporation and splash loss

The heat generated by the arc can induce the melting and evaporation of the anode and cathode. Since SnO₂ has a lower boiling point (Ag-2435 K, SnO₂-2073 K, TiB₂-3773 K), it is more prone to evaporation upon arc discharge, followed by Ag and TiB₂. Reinforcement particle agglomeration is easier to cause more evaporation loss. Verma et al^[29] thought that the splash loss of the AgMeO contact material is dominated by the thermal stability of the oxide. Rieder et al^[30] indicated that the viscosity of molten Ag significantly influences the total mass loss of AgSnO₂ and AgCdO contacts. In this work, the incorporation of TiB₂ can effectively increase the viscosity of molten Ag and reduce the occurrence of droplet splash loss, which is obviously conducive to enhancing the arc erosion resistance of the AgSnO₂TiB₂ contact material.

3 Conclusions

1) Compared with the case of the ball milling, the spatial domain-limiting effects of the template effectively improve the dispersion of the reinforcement SnO₂ and TiB₂ in the Ag matrix, which significantly increases the relative density, microhardness and conductivity of the Ag4wt% SnO₂4wt% TiB₂ contact material. The well-dispersed SnO₂ and TiB₂ can increase the viscosity of melting pool and reduce splash loss.

2) The Ag4wt% SnO₂4wt% TiB₂ contact material prepared by filter paper template presents better arc erosion resistance as compared to that by the soluble starch template method.

References

- Zhou Lei, Zhu Shiliang, Zheng Wenjia et al. *Journal of Manufacturing Processes*[J], 2020, 51: 122
- Wu Chunping, Yi Danqing, Weng Wei et al. *Materials and Design*[J], 2015, 85: 511
- Ding Jianxiang, Sun Zhengming, Zhang Peigen et al. *Materials Review*[J], 2018, 32(1): 58
- Lungu M, Gavrilu S, Nitu S et al. *Journal of Optoelectronics and Advanced Materials*[J], 2008, 10(5): 1064
- Wang Zhe, Wang Yaping. *Journal of Alloys and Compounds*[J], 2019, 774: 1046
- Wang Jun, Zhao Haidong, Wang Junbo et al. *Journal of Alloys and Compounds*[J], 2019, 770: 920
- Zhu Yancai, Wang Jingqin, Wang Haita. *Rare Metal Materials and Engineering*[J], 2013, 42(1): 149 (in Chinese)
- Wu Chunping, Zhao Qian, Li Nana et al. *Journal of Alloys and Compounds*[J], 2018, 766: 161
- Lin Zhijie, Fan Siyu, Liu Manmen et al. *Journal of Alloys and Compounds*[J], 2019, 788: 163
- Wang Junbo, Li Yingmin, Wang Yaping et al. *Rare Metal Material and Engineering*[J], 2004, 33(11): 1213 (in Chinese)
- Akbi M, Bouchou A, Zouache N. *Applied Surface Science*[J], 2014, 303: 131
- Zhang Miao, Wang Xianhui, Yang Xiaohong et al. *Transaction of Nonferrous Metals Society of China*[J], 2016, 26: 783
- Chen Z K, Witter G J. *EMBO Journal*[J], 2009(1): 182
- Qiao Xiuqing, Shen Qianhong, Zhang Lingjie et al. *Rare Metal Materials and Engineering*[J], 2014, 43(11): 2614
- Kořacz D, Księżarek S, Borkowski P et al. *Materials*[J], 2021, 14: 3297
- Zhu Yancai, Wang Jingqin, An Liqiang et al. *Rare Metal Materials and Engineering*[J], 2014, 43(7): 1566
- Liu Yanfeng, Wang Xianhui, Li Hangyu et al. *Materials Letters* [J], 2021, 293: 129 703
- Lin Zhijie, Liu Shaohong, Sun Xudong et al. *Journal of Alloys and Compounds*[J], 2014, 588: 30
- Ćosović V, Ćosović A, Talić N et al. *Journal of Alloys and Compounds*[J], 2013, 567: 33
- Fu Chong, Qiu Runhong, Zhang Yuhui et al. *Nonferrous Metals Engineering*[J], 2016, 6(6): 35
- Yang Rui, Liu Shaohong, Chen Jialin et al. *Ceramics International*[J], 2019, 45: 1881
- Wang Jinlong, Fu Chong, Li Qingxin et al. *Journal of Xi'an Polytechnic University*[J], 2020, 34(3): 61 (in Chinese)
- Li Hangyu, Wang Xianhui, Guo Xiuhua et al. *Materials and Design*[J], 2017, 114: 139
- Li Hangyu, Wang Xianhui, Xi Yong et al. *Vacuum*[J], 2019, 161: 361
- Wang Xianhui, Yang Hao, Liang Shuhua et al. *Rare Metal Materials and Engineering*[J], 2015, 44(11): 2612
- Swingler J, Sumption A. *Rare Metals*[J], 2010, 29(3): 248
- Wang Xianhui, Yang Hao, Chen Mei et al. *Powder Technology* [J], 2014, 256: 20
- Zhang Miao, Wang Xianhui, Yang Xiaohong et al. *Transaction of Nonferrous Metals Society of China*[J], 2016, 26: 783
- Verma P, Pandey O P, Verma A. *Journal of Materials Science & Technology*[J], 2004, 20(1): 49
- Rieder W, Weichsler V. *IEEE Transactions on Components, Hybrids, and Manufacturing Technology*[J], 1992, 15(3): 332

不同方法制备的AgSnO₂TiB₂电接触材料的微观结构和电弧侵蚀行为

刘彦峰^{1,2}, 王献辉¹, 何旋², 万梦豫², 苏亚宁², 叱小彤², 陈婷婷², 苗雨², 王立钊²

(1. 西安理工大学材料科学与工程学院, 陕西 西安 710048)

(2. 商洛学院化学工程与现代材料学院, 陕西 商洛 726000)

摘要: 分别采用球磨法、可溶性淀粉模板法和滤纸模板法制备了AgSnO₂TiB₂复合粉末, 并利用火花等离子体烧结技术 (SPS) 制备了块体材料。对Ag4%SnO₂4%TiB₂ (质量分数) 电接触材料的物理性能和电弧侵蚀特性进行了研究。结果表明, 模板的空间限域效应有效地改善了增强相在基体中的均匀分散, 提高了Ag4%SnO₂4%TiB₂接触材料的导电率和硬度。与球磨法相比, 滤纸模板法和淀粉模板法制备的Ag4%SnO₂4%TiB₂复合材料的电导率分别增加了12.18倍和9.60倍, 显微硬度分别增加了17.10%和33.94%。滤纸模板更有利于SnO₂和TiB₂的均匀分散, 减少集中电弧侵蚀和飞溅损失, 因此具有更好的抗弧蚀性。

关键词: 模板法; 电接触材料; 物理性能; 电弧侵蚀特性

作者简介: 刘彦峰, 男, 1982年生, 博士生, 西安理工大学材料科学与工程学院, 陕西 西安 710048, E-mail: slxylyf@126.com